

## Variability of particulate seawater properties related to bottom mixed layer-associated internal waves in shallow water on a time scale of hours

Robert Turnewitsch<sup>1</sup> and Gerhard Graf

University of Rostock, Institute of Aquatic Ecology–Marine Biology, Albert Einstein Strasse 3, D-18059 Rostock, Germany

### Abstract

To obtain information on relations between internal wave-controlled hydrographic variability in bottom mixed layers (BMLs) and particle-associated BML parameters, depth distributions of density, relative turbidity, relative chlorophyll *a* (Chl *a*), relative phycoerythrin fluorescence (Phyco), total particulate matter (TPM), particulate carbon (PC), and particulate nitrogen (PN) were obtained at a shallow-water site in the southwestern Baltic Sea in July 2001 in the course of a temporally highly resolved 1-d time series. The density distribution showed evidence for a BML and undulations of BML thickness probably caused by near-inertial internal waves. Relative pigment fluorescence in the BML and in the layer above the BML was inversely coupled and related to the wave. Dense transient PC- and PN-depleted TPM clouds, having the highest TPM loads in the BML, occurred on leading wave faces. Leading wave faces and wave backs are suggested to be locations of preferred vertical exchange between adjacent compartments (surface sediment, BML, layer above BML). Different processes control relative turbidity in the BML (decoupled from Chl *a*) and in the layer above the BML (coupled to Chl *a*). Most of the time, spatial variability of the Chl *a*/Phyco ratio was higher within the BML than in the layer above the BML. The Brunt–Väisälä frequency within the layer above the BML was positively and negatively related to the thickness of the BML and the layer above the BML, respectively. The dataset indicates that the BML itself and in coaction with passing internal waves effectively controls the communication between interior water column and sediment.

The existence of bottom mixed layers (hereafter abbreviated as BML) in near-bottom water columns has been reported for a variety of marine and freshwater environments. BMLs are usually identified by notably invariable distributions of transmission, nephels, and/or potential temperature directly above the seafloor. In the deep sea, BMLs generally exhibit a thickness of <100 m (e.g., Armi and Millard 1976; Beaulieu and Baldwin 1998; Lampitt et al. 2000), and in shallow-water systems, a thickness of a few meters (e.g., Wüest and Gloor 1998; Gloor et al. 2000). Flows over hydraulically rough beds and interactions of internal waves with the bed are the most likely reasons for BMLs to remain

active (e.g., Richards 1990; Imberger 1998). As the BML thickens, the density gradient at the upper BML boundary strengthens and inhibits further extension (Richards 1990).

It has been suggested that bottom nepheloid layers (BNLs) and their BMLs influence the biogeochemical communication between the interior ocean and the sediment (Richards 1990; Rutgers van der Loeff and Boudreau 1997; Turnewitsch and Springer 2001). Variable hydrodynamics and hydrography of the near-bottom water column (including the BML) occur on a broad range of temporal and spatial scales and may be expected to be an important trigger for changes in this communication. Besides internal tides (e.g., Ribbe and Holloway 2001), major reasons for such variability should be the occurrence of mesoscale eddies (Richards 1984), fronts (Thorpe 1983), internal waves, and a variable degree of density stratification. (Depending on the spatio-temporal scale being considered, a specific phenomenon might just be a detail of another phenomenon occurring on a larger spatiotemporal scale.) The influence of such physical phenomena on the spatiotemporal distribution of water constituents (like chlorophyll fluorescence and particulate-matter content) in the near-surface water column has been reported (e.g., Granata et al. 1995; Lennert-Cody and Franks 1999, 2002). For the near-bottom part of shallow water columns, it has been shown that, besides internal tides, internal solitary waves and seiches may trigger sediment resuspension (e.g., Gloor et al. 1994; Bogucki et al. 1997; Wang et al. 2001).

Aforementioned physical phenomena, being superimposed upon a BML, would cause variability of BML dynamics and conduct a natural experiment to study how the presence of BMLs affects (a) the communication between the interior water column and the sediment and (b) spatial heterogeneity in near-bottom water columns. In this study, we investigated

<sup>1</sup> To whom correspondence should be addressed. Present address: Southampton Oceanography Centre, European Way, Southampton SO14 3ZH, UK (rxt@soc.soton.ac.uk).

### Acknowledgments

We thank the captain and the crew of R/V *Albrecht Penck* for their very professional support and a pleasant atmosphere on board. It is a pleasure to thank Stefan Forster, Michael Friedrichs, Jörn Kleine, Elke Meier, Florian Peine, Holger Pielenz, and Kai Ziervogel, who provided invaluable help during sampling, sample processing, and analysis and who created an unforgettably good working atmosphere. Multicorer, Bottom Water Sampler, and the excellently equipped and maintained CTD rosette were provided by the Baltic Sea Research Institute in Warnemünde (IOW; Stefan Forster, Harry Becher, and Henry Will). Bernd Kayser (IOW) converted the CTD files. The enlarged map in Fig. 1 was provided by Björn Bohling (IOW) using the dataset from Seifert and Kayser (1995). We thank Hans-Ulrich Lass, two anonymous reviewers, and the associate editor for very constructive comments and suggestions that improved this manuscript. The financial support of the Bundesministerium für Bildung, Wissenschaft, Forschung und Technologie (DYNAS project; contract No. 03F0280B) is gratefully acknowledged.

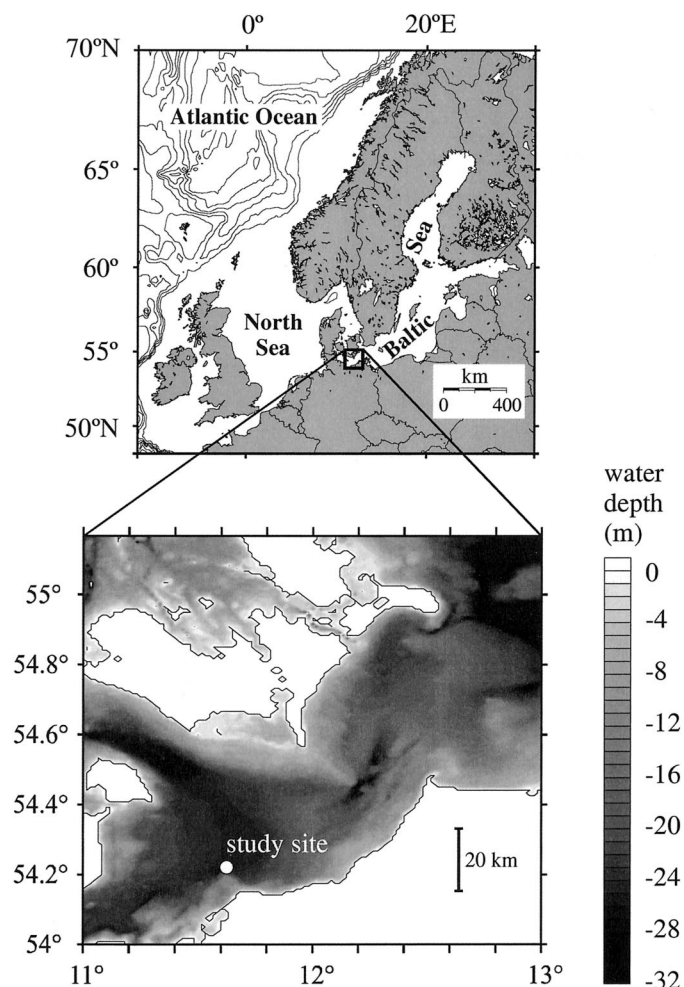


Fig. 1. Map of the location of the study site. The enlarged map shows the approximate bathymetry of the area surrounding the study site (map obtained from the dataset provided by Seifert and Kayser [1995]).

relationships between internal wave-controlled hydrographic variability and variability in distributional and compositional particulate-matter characteristics within the BML to help illuminate this proposed BML “filter.”

## Material and methods

**Study area**—The study area is part of the Mecklenburg Bay in the western Baltic Sea (Fig. 1) and is located at the western end of the ‘Western Baltic Sea–Gulf of Finland’ seiche system (Magaard 1974). In this region, meteorological seasonality of the wind and air-temperature regime is reflected in a pronounced seasonality of the hydrography and in the biological and biogeochemical characteristics and functioning within the water column and sediment (e.g., Siedler and Hatje 1974; Smetacek et al. 1978; Smetacek 1980; Graf 1992). From early spring until early autumn, the water column exhibits a stable density stratification. During spring, summer, and/or autumn, fluffy and easily resuspended particulate matter may partly or completely cover larger

areas of the sediment surface in this region. Tidal influence is negligible (Magaard 1974).

**Methods**—Profiles of hydrographic and optical water characteristics and water and sediment samples were collected during R/V *Albrecht Penck* cruise 40/01/15 on 5/6 July 2001 at a coastal site (station No. 237000; 54.224°N, 11.621°E; water depth ~26.5 m) of the western Baltic Sea (Fig. 1). The ship anchored during time-series sampling (1.2 d; temporal resolution ~30 min). The ship’s draught is ~3 m and could have affected properties of the surface mixed layer. However, this part of the water column was of minor importance for this study. Temperature, salinity, and pressure were measured with a Seabird Electronics SBE 911+ CTD (conductivity, temperature, depth) deployed midship and equipped with a rosette of bottles for sampling water. Relative chlorophyll *a* and phycoerythrin fluorescence (hereafter abbreviated as Chl *a* and Phyco, respectively; values shown are voltages) and relative turbidity were determined with an integrated Backscat II-fluorometer (Dr. Haardt Optik Mikroelektronik, model 1303 MP/Chla/Phy/2R/MO). Phycoerythrin is a light-harvesting phycobiliprotein common in cyanobacteria, rhodophytes, and cryptophytes (Jeffrey 1997; Jeffrey and Vesk 1997). Pigment fluorescence and turbidity were measured within the same volume of seawater (typically 0.1 ml). The optical sensors operate independently of daylight. The turbidity sensor measures the part of the emitted flashlight backscattered to about  $175 \pm 5$  degrees by the particulate material in the water. There is practically no influence of absorption by dissolved substances. However, the sensitivity of the sensor is about one order of magnitude higher for mineral particles than for organic ones. The turbidity sensor is calibrated in relative reflectance units (Dr. Haardt Optik Mikroelektronik 1996). Water inlet for temperature and salinity sensors and pressure and optical sensors were mounted close to each other within the rosette frame. A calibrated Log Quantum Scalar Irradiance Sensor (QSP-200L; Biospheric Instruments) for the measurement of photosynthetically active radiation (PAR) was mounted on top of the CTD frame ~1.2 m above the other sensors. Water above the first meter above bottom was sampled with gray polyvinyl chloride (PVC) bottles attached to the CTD rosette frame. The bottoms of the bottles were shaped to allow complete clearance of bottle contents via the spigot (see Gardner 1977). An acoustic altimeter monitored the distance between the CTD sensor package and the seafloor. Vertical spatial resolution of sensor sampling was approximately 0.1 dbar. Water was sampled at four different heights within the first meter above bottom (0.1, 0.2, 0.3, and 0.4 m) with a specially designed bottom water sampler (BWS). Water was collected by the BWS approximately 30 min after ‘touch down’ to minimize the risk of biased results due to material that was resuspended during touch down. All water samples were drained into containers and gently mixed within the containers before filtration (see below for more details). To avoid biased water-column data due to artificial resuspension, sediment samples were obtained at the end of the water-column time series. These virtually undisturbed sediment samples were taken with a multiple corer (modified after Barnett et al. 1984) to avoid loss of the easily resuspended fluffy layer

on the sediment surface. Fluffy material from the sediment surface was carefully sampled with a plastic syringe, transferred to a plastic bag that was heat sealed, and stored frozen ( $-20^{\circ}\text{C}$ ) and in the dark until analysis (see below). The ship's instruments continuously monitored meteorological parameters.

Water collected for total particulate-matter (TPM), particulate carbon (PC), and particulate nitrogen (PN) analyses was filtered using precombusted ( $500^{\circ}\text{C}$  overnight), preweighed glass-fiber Whatman GF/F filters (nominal pore width  $0.7\ \mu\text{m}$ ) on a gray PVC filtration device at approximately  $-200$  mbar low pressure. To avoid methodological bias due to use of different volumes of filtered water and/or different filter diameters (unpublished data), for all samples, 1 L of water (measured in a volumetric flask) was filtered within less than 1 h after sampling using 25-mm-diameter filters. Until analysis, TPM filters were stored in plastic containers, frozen ( $-20^{\circ}\text{C}$ ) and in the dark. TPM filters and fluff subsamples from the sediment surface were dried overnight at  $60^{\circ}\text{C}$ , cooled off in a desiccator, and weighed. They were then stored in the desiccator until analysis for PC and PN conducted with a Carlo Erba NA-1500 analyzer (Verardo et al. 1990) using acetanilid standards. To roughly assess potential methodological bias caused by adsorption of dissolved organic material onto the filters,  $0.7\text{-}\mu\text{m}$ -prefiltered water was filtered once again. PC, PN, and TPM loads determined for those filters were used as background values and subtracted from PC, PN, and TPM values determined for the sample filters.

## Results

A persistent BML, exhibiting a thickness of 5–6.5 m, was observed in the density distribution. A pycnocline (between 20 and 21 dbar) covered the BML during the whole time series (Fig. 2a,b). This pycnocline exhibited approximately two undulations within 24 h and a wave height of  $\sim 1.5$  m (Fig. 2b).

Below a depth of 17 dbar, relative turbidity decreased toward 22–23 dbar, reaching minimum values (Fig. 2c,d). Below this depth, turbidity increased again toward the seafloor. Some profiles indicate that, within the lower part of the BML (as defined by density distribution), turbidity remained virtually constant (Fig. 2c). This part of the turbidity profiles reflected the same qualitative variability of BML thickness as the density distribution (Fig. 2d). However, the vertical BML extension as indicated by turbidity distributions was less than the BML extension as indicated by density distributions (cf. Fig. 2a,c).

Below the main maximum of Chl *a*, which was centered around 15 dbar, Chl *a* decreased rapidly toward the BML pycnocline (Fig. 3a). Within this near-bottom pycnocline, Chl *a* increased again and a clear secondary persistent Chl *a* maximum was observed which was, however, much narrower and less pronounced than the main maximum around 15 dbar (Fig. 3a,b). The vertical location of the peak of this secondary maximum followed BML pycnocline undulations (Fig. 3b). Below this secondary maximum, Chl *a* was almost invariable, approximately reflecting the vertical extension of

the BML as defined by the density distribution (see Figs. 2b, 3b). Phyco (data not shown) exhibited the same major distributional features as Chl *a*. Below the main maximum of Chl *a*, the ratio of Chl *a*/Phyco decreased toward the seafloor (Fig. 3c). Most of the time, spatial variability of this ratio was higher within the BML than in the layer between the main Chl *a* maximum and the BML pycnocline (the “layer above the BML”; Fig. 3c,d).

The TPM dataset as a whole (except for four profiles; see below) reflects the major distributional features of relative pigment fluorescence and turbidity (see Figs. 2c, 3a, 4a). The increase of turbidity toward the seafloor within the BML (as defined by density distribution), however, is not reflected in the TPM data (see Figs. 2c, 4a). TPM profiles obtained on 5 July at 2155 h (CTD 15) and on 6 July at 0925, 1110, and 1240 h (CTDs 38, 42, and 45, respectively) are vastly different as compared with the rest of the TPM profiles: Within similar depth ranges, TPM values generally were at least twice as high ( $>2\ \text{mg L}^{-1}$ ) as in the other TPM profiles (usually  $<2\ \text{mg L}^{-1}$ ), and TPM increased almost linearly from the sea surface ( $\sim 2\text{--}3\ \text{mg L}^{-1}$ ) toward the seafloor ( $\sim 6\text{--}8\ \text{mg L}^{-1}$ ) (Fig. 4a). These peculiar TPM distributions were not reflected in turbidity or pigment fluorescence (see Figs. 2c, 3a, 4a,b). Moreover, samples from the peak of pigment fluorescence within the BML pycnocline form a separate cloud of data comprising comparatively high TPM values at lowest turbidity (Fig. 4b). Both PC and PN showed the lowest concentrations below the Chl *a* maximum, somewhat higher values above, and the highest concentrations within and directly above the Chl *a* maximum (data not shown). PC and PN data obtained from the four peculiar CTD hauls mentioned above exhibited the same trends but higher values. Molar C/N ratios were between 7 and 9 above the Chl *a* maximum and between 6 and 9 below the Chl *a* maximum (data not shown). PC/TPM ratios (most values between 5 and  $100\ \mu\text{mol PC/mg TPM}$ ) and PN/TPM ratios (most values between 0.7 and  $10\ \mu\text{mol PN/mg TPM}$ ) usually decreased toward the seafloor (Fig. 4c,d). The TPM profiles exhibiting unusually high TPM values as mentioned above were characterized by notably low PC/TPM and PN/TPM data. Fluffy material collected from the sediment surface was characterized by molar C/N ratios of 7.3–8.8 and by PC/TPM and PN/TPM ratios of 3.7–4.2  $\mu\text{mol PC/mg TPM}$  and 0.48–0.51  $\mu\text{mol PN/mg TPM}$ , respectively (Fig. 4c,d).

## Discussion

*Internal waves*—To facilitate the discussion of relationships between internal wave-controlled hydrographic variability and variability in particulate-matter characteristics, wave types and their influence on near-bottom hydrodynamics will be the subject of this first section of the discussion. Given the wave period (12–13 h), the observed hydrographic undulation might have been due to a third-order internal undulation of the Western Baltic Sea–Gulf of Finland seiche system (Magaard 1974). A more likely reason for the observed undulation, however, is the occurrence of internal near-inertial waves (the theoretical period of inertial oscillations at this latitude is  $14.8\ \text{h} = 12\ \text{h}[\sin 54.224^{\circ}]^{-1} =$

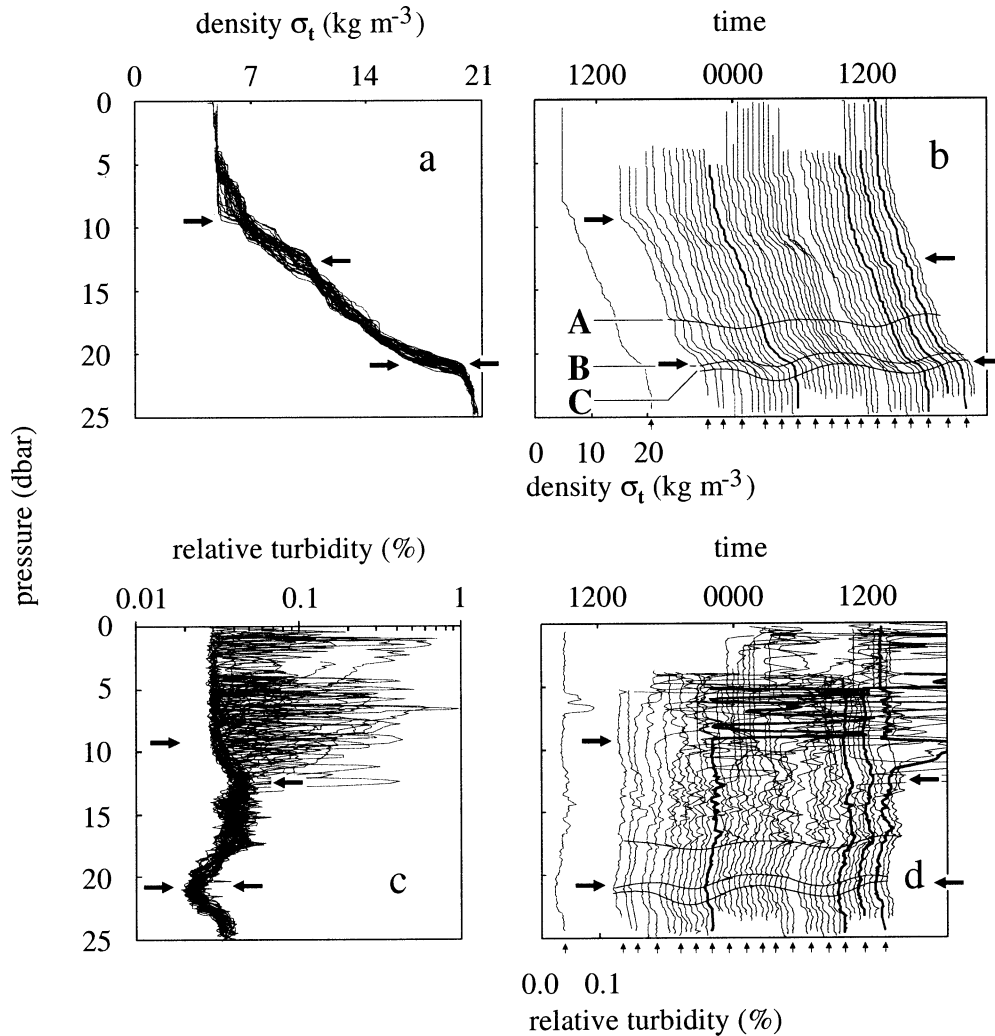


Fig. 2. Depth distributions of (a, b) density and (c, d) relative turbidity. The figures on the left-hand side show all profiles of the time series superimposed on each other to illustrate the range of values at each depth. Figures on the right-hand side show profiles as a time series; for each profile, the point of reference with respect to time is the data point closest to the sea surface; the lower abscissa applies only to the first profile of the time series. Thick horizontal arrows indicate the location of the two principal pycnoclines at the beginning and at the end of the time series. Undulating lines in figures on the right-hand side indicate the approximate location of the upper boundary of (A) the layer between the BML pycnocline and the lower boundary of the main chlorophyll *a*-fluorescence maximum, of (B) the BML pycnocline, and of (C) the BML. The layer denoted “the layer above the BML” in the text is confined by line A and the secondary chlorophyll *a*-fluorescence maximum within the BML pycnocline (see Fig. 3a,b). Vertical arrows at the lower abscissa mark CTD deployments that included bottle sampling of water. Bold profile lines indicate CTD deployments exhibiting notably high amounts of filtered total particulate matter (see Fig. 4). Some extremely high peaks in (d) are not fully depicted.

$2\pi f^{-1}$ ; also see Krauss 1974, his fig. 1). Two transient increases of air pressure, being superimposed on an overall drop in air pressure (Fig. 6a), coincided with the BML wave’s leading face and may also have had an effect on the formation of the internal wave. The wave amplitude ( $\sim 0.7$ – $0.8$  m) of the BML pycnocline approximately equaled 1/10 the BML thickness ( $\sim 5$ – $6.5$  m) and was much less than  $\sim 1/10$  total water depth (26.5 m). Therefore, the observed near-bottom internal wave approximately resembles an idealized long linear interfacial near-inertial internal wave (see,

e.g., Lennert-Cody and Franks 1999, their fig. 3a). Because waves of the aforementioned period usually have wavelengths that exceed the water depth, they “feel” the seafloor and can induce energetic disturbances within the near-bottom water column.

The idealized movement of water due to a long near-bottom linear interfacial internal wave is outlined in Fig. 6d. Due to a maximum separation of wave-related streamlines in a layer of maximum thickness, wave-related horizontal motions are expected to be least vigorous at maximum layer

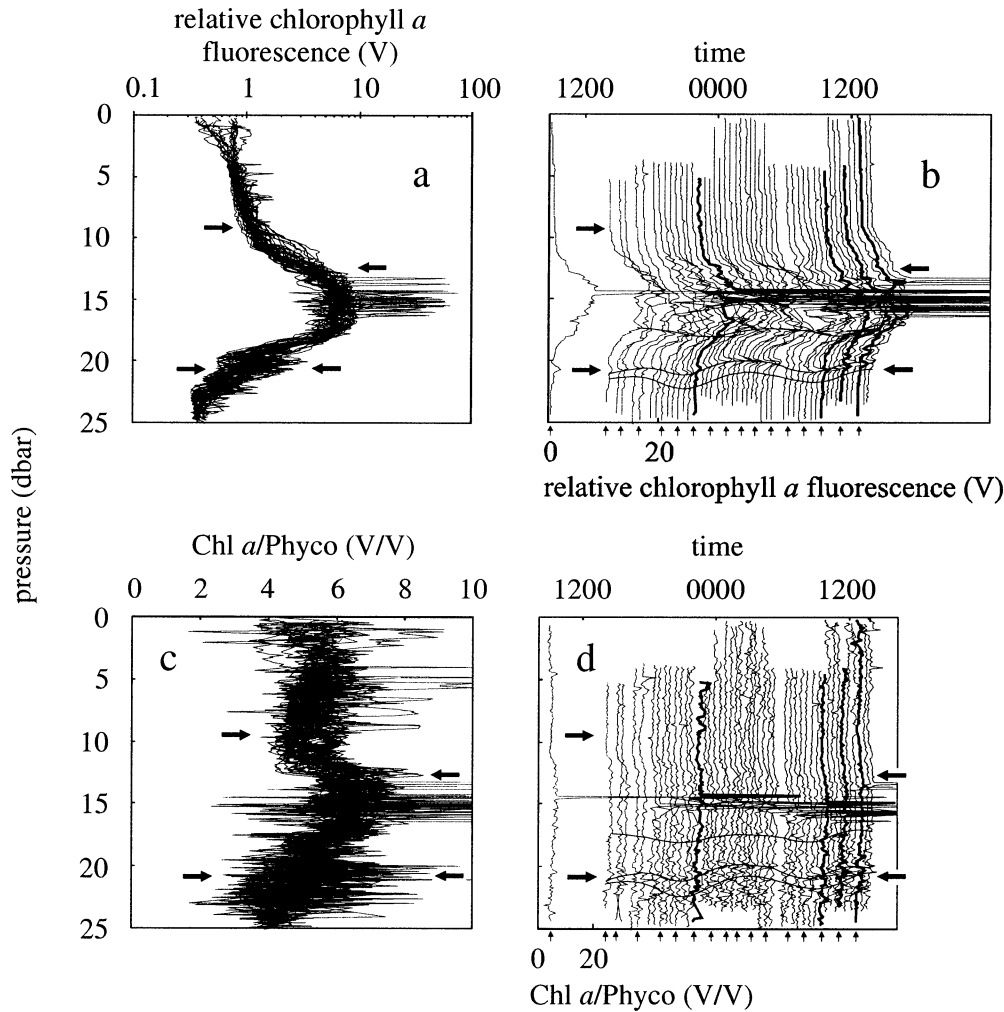


Fig. 3. Depth distributions of (a, b) relative chlorophyll *a* fluorescence (Chl *a*) and (c, d) the ratio of relative chlorophyll *a* fluorescence and relative phycoerythrin fluorescence (Chl *a*/Phyco). More detailed information on the structure of the diagrams can be found in the caption of analogous Fig. 2.

thickness, and vice versa. In the BML wave trough wave-related transport of water is chiefly horizontal (Fig. 6d). Here wave-related horizontal streamlines are closer to each other than in any other part of the BML wave, illustrating enhanced horizontal current velocities and suggesting increased vertical shear-induced instability of the BML. Above the BML wave trough, the wave-related current direction is reversed and the separation of streamlines reaches maximum values, suggesting less vigorous hydrodynamic conditions. On the BML wave's leading face, internal wave-related water motions are directed upward and across the BML pycnocline, forming a convergence within the BML and a divergence within the layer above the BML (i.e., the layer confined by line A and the BML pycnocline between lines B and C in Fig. 2b). Vertical velocities are maximal at the interface (Lennert-Cody and Franks 1999; Fig. 6d). In the BML wave crest, horizontal wave-induced currents prevail again but, in comparison with the BML wave trough, the wave-associated current direction reverses by 180° (Fig. 6d). Wave-related velocities point to opposite directions in the

BML and in the layer above the BML. Due to a thickening BML, the distance between adjacent streamlines increases (Fig. 6d) and wave-related horizontal current velocities are not as strong as in the BML wave trough. If wave-related currents and background currents in the BML point to opposite directions, the BML becomes even less dynamic under the wave crest. Compared with the BML wave-trough area, the difference in the separation of streamlines between the BML and the layer above the BML is less pronounced, i.e., wave-related current velocities in the BML are reduced and velocities in the layer above the BML are enhanced. On the BML wave back behind the BML wave crest, wave-related water transport is directed downward, forming a divergence in the BML and a convergence in the layer above the BML (Fig. 6d). Again, vertical velocities are maximal at the BML pycnocline.

*Total particulate matter versus relative turbidity*—Before returning to relationships between internal waves and particulate matter, the explanatory power of the measured particle-

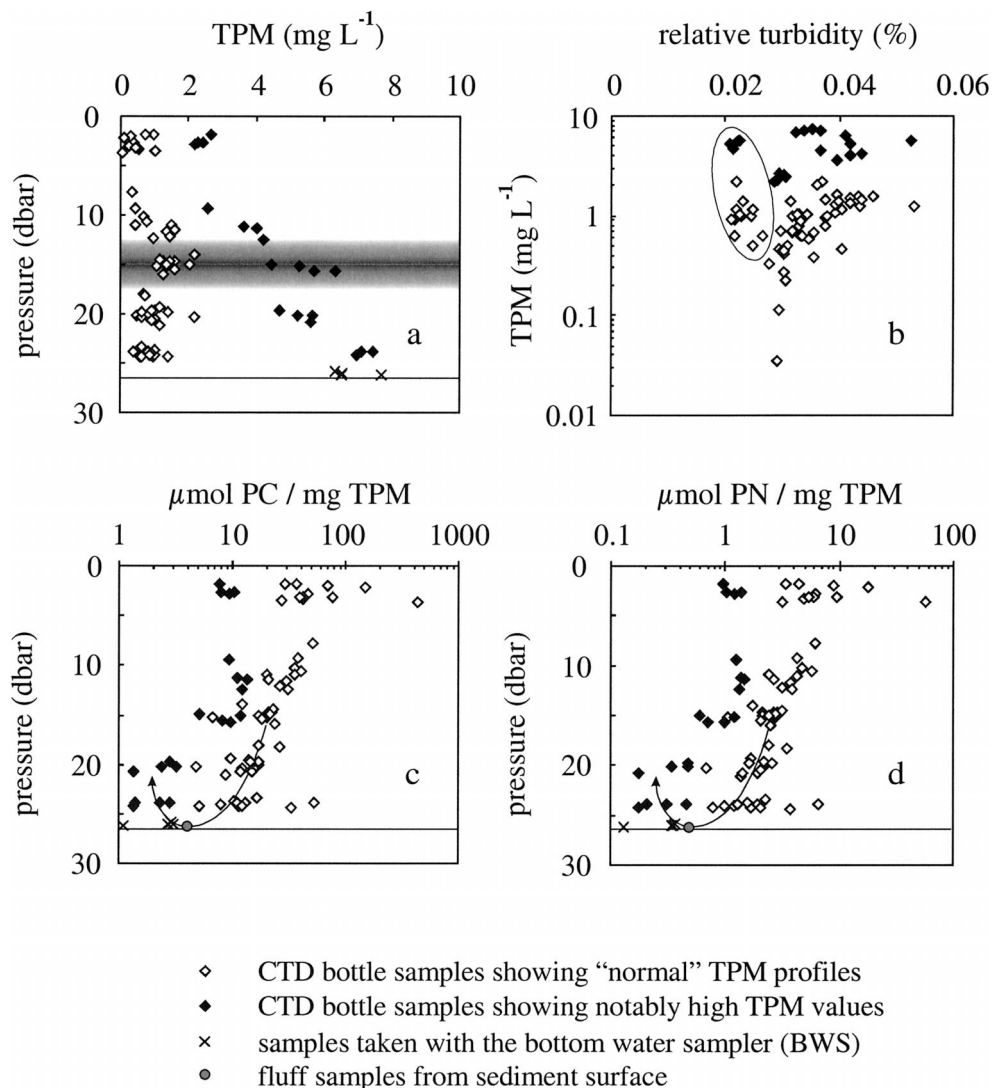


Fig. 4. (a) Complete dataset of depth distribution of filtered total particulate matter (TPM). (b) Plot of TPM versus relative turbidity, which was measured directly below the sampling bottle when the bottle was closed (encircled data were obtained from the Chl *a* peaks within the BML pycnocline; cf. Fig. 3b). (c, d) Depth distribution of the ratios (particulate carbon contents)/(TPM contents) and (particulate nitrogen contents)/(TPM contents), respectively. Closed diamonds indicate data originating from CTD profiles indicated by bold lines in the time-series plots of Figs. 2 and 3. The gray area in (a) marks the location of the main Chl *a* maximum. Horizontal lines in (a), (c), (d) indicate depth of the seafloor. Bent arrows in (c) and (d) indicate the proposed changes of the PC/TPM and PN/TPM ratios during TPM ageing (see Discussion).

related parameters will be briefly discussed. There was no simple relationship between TPM mass concentration and relative turbidity: (a) Notably high TPM values of four CTD casts are not reflected in equally enhanced relative turbidities (Figs. 2c,d, 4a,b). (b) Data from the peak of pigment fluorescence that occurred within the BML pycnocline form a separate cloud of data comprising comparatively high TPM values at lowest turbidity (Fig. 4b). (c) Very high transient and spatially narrow peaks of relative turbidity that occurred within the whole water column above the main Chl *a* maximum were never reflected in TPM data (Figs. 2c,d, 4a). These results show that the optical-sensor and the filter approach for quantification of particulate-matter concentration

have different sensitivities for different kinds of particles. What are possible reasons for this discrepancy? Relative turbidity was assessed by measuring backscattering of emitted light by the particulate material. Measurement of backscattering is more sensitive to mineral particles than to organic ones, the ratio of sensitivity to mineral particles or particles with a mineral shell being about one order of magnitude higher compared with that of organic particles. Moreover, GF/F filters have a nominal pore width of 0.7  $\mu\text{m}$ . Thus, the filter approach ideally detects all particles  $>0.7 \mu\text{m}$ , whereas the optical sensor preferentially detects a specific fraction of the whole particle spectrum. Another source of discrepancy arises from the fact that the filter approach integrates over a

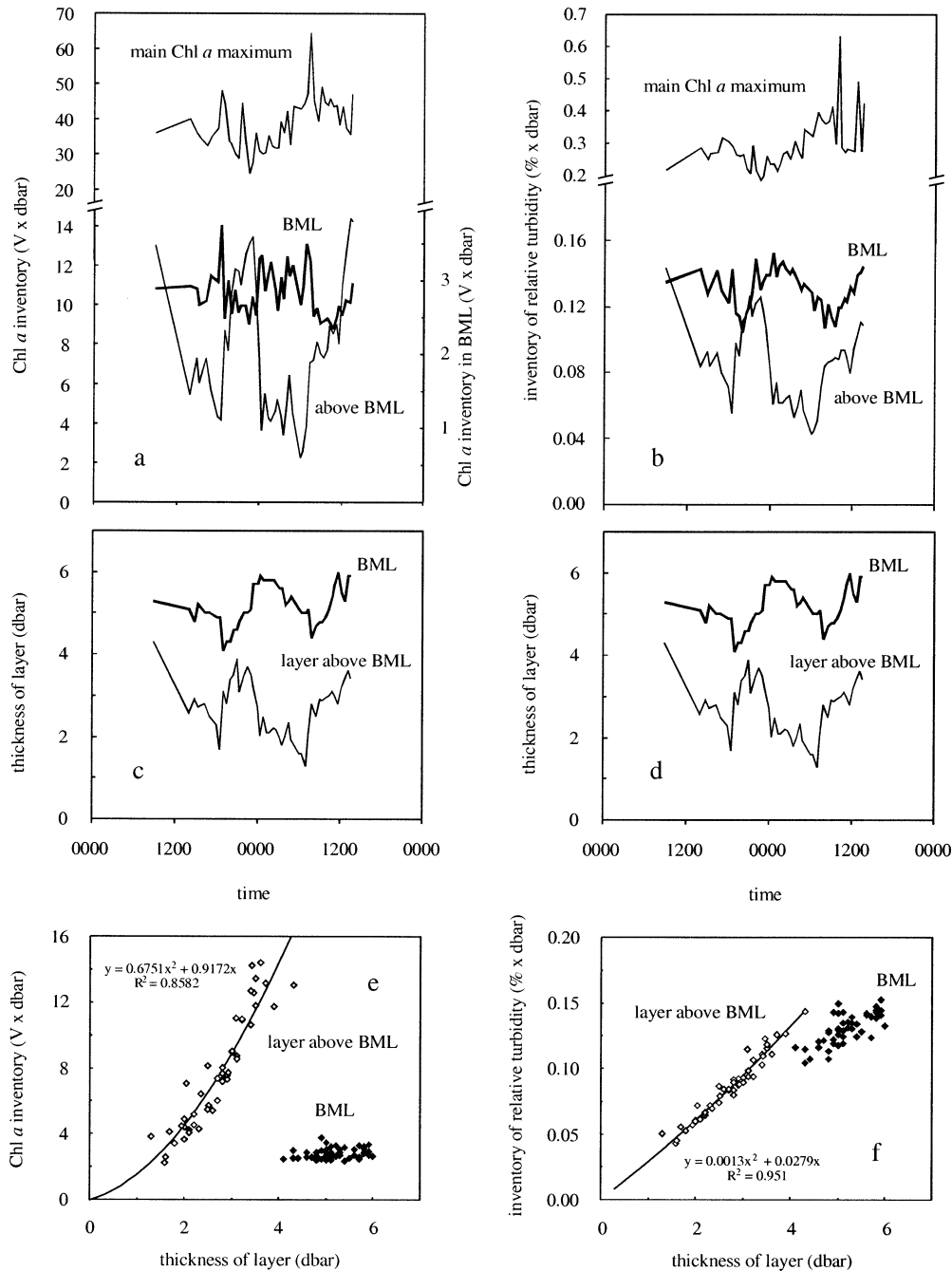


Fig. 5. Time series of inventories of (a) Chl *a* and (b) relative turbidity in the main Chl *a* maximum, the layer above the BML, and the BML. For each layer, inventories have been calculated by trapezoidal integration. (c, d) Time series of the thickness of the BML and the thickness of the layer above the BML. Both diagrams are identical and were plotted to facilitate the allocation of changes of inventories of Chl *a* [in (a)] and relative turbidity [in (b)] to wave-related changes of layer thickness. (e, f) Relationships of inventories of Chl *a* and relative turbidity to the thickness of the BML and the thickness of the layer above the BML.

water volume of 1 L (here 1 L subsampled from a well-mixed volume of ~5 L of seawater completely drained from the CTD-rosette bottles) whereas the turbidity sensor typically samples a volume of 0.1 ml. This complex of considerations shows that the filter approach has an increased sensitivity for rarer and larger particles (aggregates) as

compared with the turbidity sensor, which is more reliable for the detection of smaller particles having a higher reflectance and being more abundant than the aforementioned aggregates. Hence, very high TPM values, not being reflected in sensor-derived data, will be viewed as a qualitative measure for the abundance of aggregates throughout the follow-

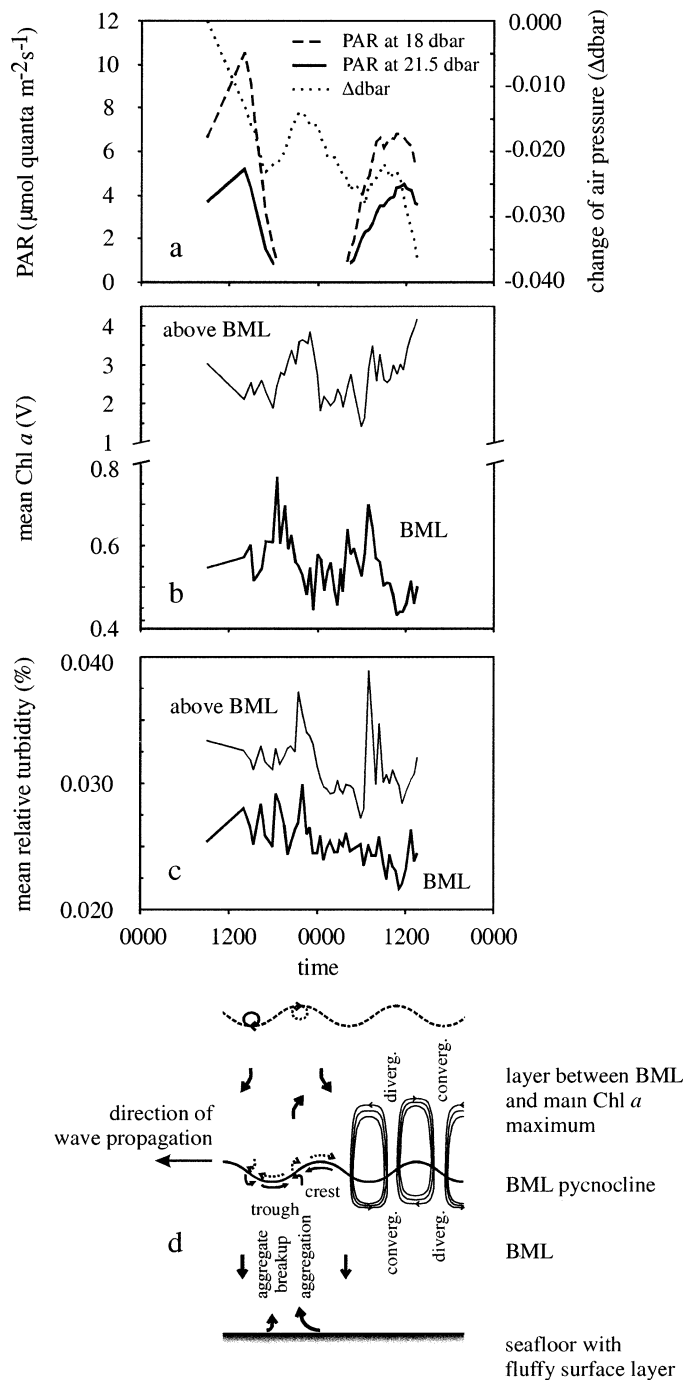


Fig. 6. (a) Time series of the intensity of photosynthetic active radiation (PAR) at 18 and 21.5 dbar and of the change of air pressure relative to the start of the time series. (PAR intensities below  $\sim 1 \mu\text{mol quanta m}^{-2} \text{s}^{-1}$  are close to the minimum reliable irradiance value of  $\sim 0.5 \mu\text{mol quanta m}^{-2} \text{s}^{-1}$  [Biospherical Instruments 1993] and have been omitted.) (b, c) Time series of mean relative turbidity and mean relative chlorophyll *a* fluorescence in the BML and in the layer above the BML. Values were calculated by dividing the respective inventory ( $\% \times \text{dbar}$  and  $\text{V} \times \text{dbar}$ ; see Fig. 5a,b) by the thickness of the layer (dbar). (d) Left-hand side: Conceptual model of water motions induced by internal waves (thin arrows and circles) and their proposed influence on particulate-matter (aggregate) dynamics within the near-bottom water column (thick arrows). Right-hand side: Conceptual sketch of the linear interfacial internal

ing discussion. Relative pigment fluorescence (Chl *a* and Phyco) and relative turbidity will be used as proxies for largely suspended more organic and more anorganic material, respectively. (Also see Leipe et al. [2000] for more information on particulate-matter composition in the coastal southwestern Baltic Sea.)

*Internal waves and particle transport and dynamics*—If there were no net transport of particles relative to wave-related water movements, no particle input to and no particle loss from the BML, and no significant changes in relative abundance of different categories of particles, mean concentrations within the BML would not change over the wave cycle (Lennert-Cody and Franks 1999). Consequently, BML inventories of the respective constituent would be linearly and positively related to BML thickness (i.e., the size of the compartment). The same is true for the layer above the BML. In fact, inventories of Chl *a* and relative turbidity within the layer above the BML, and the inventory of relative turbidity within the BML exhibited a clear positive relationship to the thickness of the respective layer (Fig. 5a–f). However, there was no linear relationship between inventories of Chl *a* and relative turbidity on the one hand and the layer thickness of the layer above the BML on the other hand (Fig. 5e,f). Moreover, the inventory of Chl *a* in the BML showed much less temporal variability and no obvious positive relationship to BML thickness (Fig. 5a,e). Instead, and despite the low overall variability in the BML, there was evidence for a clear-cut opposite behavior of the BML Chl *a* inventory when compared with temporal fluctuations of the Chl *a* inventory in the layer above the BML (Fig. 5a). There is some evidence for a linear relationship between the inventory of relative turbidity in the BML and BML thickness (Fig. 5f). There was a slight phase shift between wave-associated variability of layer thickness in the BML and in the layer above the BML (Fig. 5c,d: the BML lagged by  $\sim 90^\circ$  relative to the layer above the BML).

These findings have several implications: (1) In addition to mere wave-associated transport, other processes indirectly controlled by the waves must be invoked to explain the observed distributional patterns of particulate-matter parameters. (2) Chl *a* in the BML is inversely coupled to Chl *a* in the layer above the BML and controlled by wave-related processes occurring in the layer above the BML. (3) Two different processes control relative turbidity in the BML (decoupled from Chl *a*) and in the layer above the BML (coupled to Chl *a*). These notions are reflected in the fact that temporal changes of mean Chl *a* and mean relative turbidity (indicating changes of concentration) were observed in the layer above the BML and of Chl *a* also within the BML (Fig. 6b,c). In the layer above the BML, increased mean Chl *a* and relative turbidity occurred when layer thickness and

wave-related stream function indicating the location of divergences and convergences (adapted from Lennert-Cody and Franks 1999, their fig. 3a). The conceptual model is vertically not to scale but was horizontally (temporally) scaled to resemble the observed wave period.

Chl *a* inventories were high as well. This happened on the BML wave's leading face. In contrast, in the BML, mean Chl *a* was increased in the BML wave trough (cf. Figs. 5, 6b,c). Mean relative turbidity in the BML did not show any clear systematic fluctuations (Fig. 6c).

Thus, for continuity reasons, the temporal wave-related changes of mean Chl *a* and mean relative turbidity in the layer above the BML and of mean Chl *a* in the BML also indicate that, besides wave-induced transport of passive particles, other processes, indirectly controlled by wave dynamics, must have contributed to the formation of these observed particle-associated spatiotemporal patterns. At this stage, the search for key processes determining those patterns has to remain speculative. However, assuming backgrounds (i.e., without the effect of internal waves) of vertical and horizontal turbulent diffusivity, settling behavior of particles, and lateral advection to be spatiotemporally constant across the internal-wave field, the following wave-affected processes should be likely candidates.

(1) Net input from and net removal to adjacent compartments by wave-induced resuspension, gravitational settling, and/or turbulent-diffusive or advective transport—for example, on the BML wave's leading face, at least two results support the notion that processes involving the surface sediment (resuspension) control the formation of the transient TPM clouds: (a) Values for PC/TPM and PN/TPM ratios in fluffy particulate material sampled from the sediment surface are between the respective ratios observed on the leading wave face and on the other parts of the wave (Fig. 4c,d); this suggests that aggregates, which partially degrade while settling from the interior water column toward the seafloor (decreasing PC/TPM and PN/TPM ratios), are resuspended as the wave's leading face approaches and undergo further aging in (re)suspension on the wave's leading face (as reflected in a further decrease of PC/TPM and PN/TPM ratios in the near-bottom water column; Fig. 4c,d). (b) The linear TPM increase toward the seafloor on the BML wave's leading face (Fig. 4a) also suggests that the source of this material is situated at or close to the seafloor. Another example can be found on the wave back. On the wave back, the wave-induced downward movement of water adds to gravitational particle settling. Hence, particles (re)settle more easily as reflected in the absence of notably high TPM values and in decreased mean relative turbidity and pigment fluorescence in the layer above the BML. Leading wave faces and wave backs should therefore be locations of preferred vertical exchange between adjacent compartments (surface sediment, BML, layer above BML).

(2) Particle breakup and aggregation causing a shift among the different particle size classes and a change of relative sensitivities of different approaches to quantify particulate-matter loads in the water—for example, increased mean Chl *a* in the BML wave trough (Fig. 6b) may have resulted from aggregate breakup in the hydrodynamically more vigorous environment of the wave trough. Another example occurred on the BML wave's leading face: The wave-related convergence in the BML tends to bring particles closer together, facilitating particle encounter and aggregation as reflected in considerably increased amounts of TPM.

(3) Directional swimming of planktonic organisms (see Lennert-Cody and Franks 1999, 2002).

*Internal waves or (photo)chemical and biogeochemical reactions?*—Light (PAR) intensity also varied during this time series. Could (photo)chemical reactions have caused the observed patterns? Light intensities within the studied near-bottom water column (usually  $<10 \mu\text{mol quanta m}^{-2} \text{s}^{-1}$ ; Fig. 6a) were low enough to justify the assumption that this part of the water column was close to the compensation depth (light intensities usually  $3\text{--}30 \mu\text{mol quanta m}^{-2} \text{s}^{-1}$ ). The compensation depth defines the lower boundary of the euphotic zone and the area of the water column where photosynthetic production is balanced by plant respiration. It is, therefore, safe to assume that biogenic particulate organic matter in the studied near-bottom water column was not directly influenced by diel changes in net photosynthetic production and other related parameters (see, e.g., Cullen and Lewis 1988).

Incident light intensities have been shown to affect a number of phytoplanktonic parameters (e.g., quantum yield of fluorescence, fluorescence/chlorophyll *a* ratios, mean fluorescence per cell, pigment ratios, growth rate; see, e.g., Kiefer and Reynolds 1992; Moore et al. 1995; Oliver and Whittington 1998). For some organisms and parameters, the effect is most pronounced when light intensity varies within the low-intensity range ( $<20 \mu\text{mol quanta m}^{-2} \text{s}^{-1}$ ) that is relevant to this study (e.g., Moore et al. 1995, their figs. 4, 7a,b, 9). However, the period of changes in light intensity (24 h) was about twice as long as the period for changes in particulate matter (12–13 h) and for some particle-associated parameters it was also phase-shifted. Hence, variable light intensity is unlikely to be a major reason for the observed changes in particulate matter. The absence of clear and systematic Chl *a*, TPM, and turbidity fluctuations within the main Chl *a* maximum (Fig. 5a,b) indicates that near-bottom patterns have not been controlled profoundly by rapid downward transfer of light-controlled diel patterns within the upper water column (through particles settling at velocities  $>30 \text{ m d}^{-1}$  being typical for particles constituting the bulk of particle-associated downward fluxes in the ocean; see, e.g., Fowler and Knauer 1986).

Decomposition of complex natural organic material and dissolution of minerals usually take place on time scales of weeks or longer (e.g., Middelburg 1989; Grossart and Ploug 2001; Rickert et al. 2002) and therefore cannot explain the observed variability in pigment fluorescence, turbidity, and TPM concentration having occurred on time scales of hours. This also implies (1) that the proposed process of TPM aging in the near-bottom water column must be based on considerably enhanced residence times of TPM in the near-bottom water columns of the wave's leading face and (2) a "sweeping" effect of the BML wave's leading face. This, in turn, supports the idea of a spatiotemporally more extensive and longer lived wave field.

*BML: A filter between sediment and interior water column*—BML hydrodynamics differ from hydrodynamics within the interior water column (e.g., Richards 1990). The pycnocline covering the BML is the detectable boundary

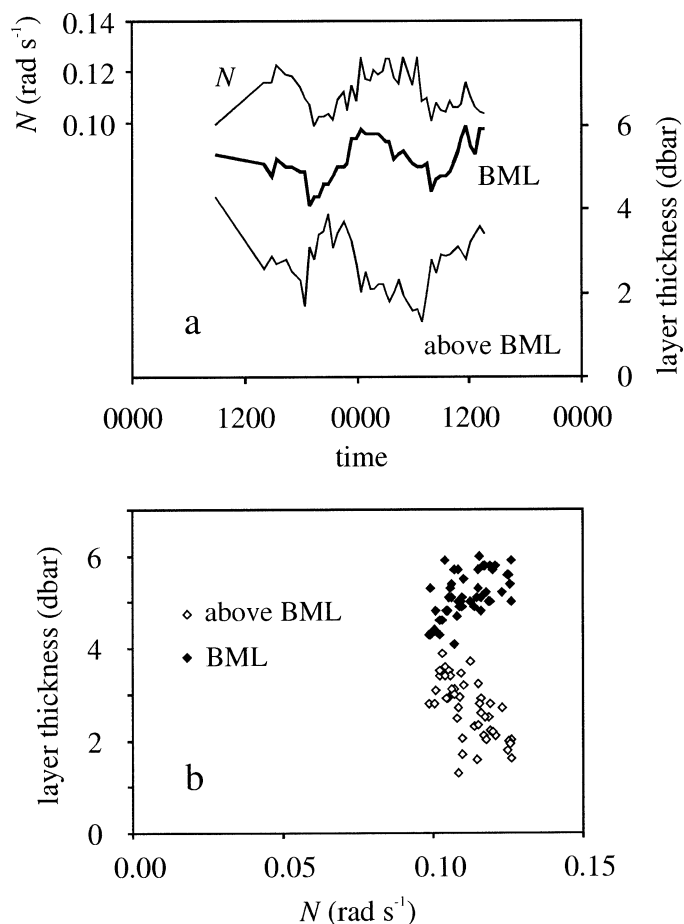


Fig. 7. (a) Time series of the Brunt-Väisälä frequency ( $N = (g/\rho \, d\rho/dz)^{0.5}$ ) within the layer above the BML in comparison with the time series of the thickness of the BML and the thickness of the layer above the BML;  $g$  = acceleration due to gravity,  $\rho$  = density of seawater,  $z$  = thickness of the layer above the BML. (b) Relationships between the Brunt-Väisälä frequency ( $N$ ) within the layer above the BML and the thickness of the BML and the thickness of the layer above the BML.

between these compartments of the water column and, through enhanced stratification and stability, inhibits exchange between both compartments. Increased values of the Brunt-Väisälä frequency ( $N$ ) within the layer above the BML during passage of the BML wave crest and maximum BML thickness support this notion (Fig. 7a,b). (Due to the near-inverse behavior of the BML and the layer above the BML, the relationship between their layer thicknesses and  $N$  is also reversed [Fig. 7b].) It is worthwhile noting that the difference between the BML and the interior water column is not only discernible in physical data but also in particle-related data: (a) The maximum of pigment fluorescence in the BML pycnocline exhibits maximal values on the BML wave crest (Fig. 3b), supporting the idea of an especially strong stratification within the BML pycnocline during passage of the BML wave crest and stressing the BML's role as a barrier. (b) Processes controlling relative turbidity differ in the BML and in the layer above the BML (see above). (c) A peculiar and yet unexplainable enhancement of spatial var-

iability of the Chl *a*/Phyc ratio was observed in the BML (see Fig. 3c,d; at this study site, resuspended rhodophyte debris is one possible reason for enhanced spatial heterogeneity of this ratio within the BML).

Despite the short duration of the time series, the internal consistency of the dataset (a) accentuates the considerable spatiotemporal biogeochemical complexity of coastal stratified water columns resulting from the superposition of a multitude of physical, sedimentological, biological, and biogeochemical processes; (b) suggests that linear near-inertial internal interfacial waves might provide important mechanisms that control the linking and interplay of those processes; and (c) indicates that the BML itself and in coaction with passing internal waves effectively controls the biogeochemical communication between the interior water column and the sediment. More systematic multidisciplinary studies are required to advance the understanding of the nature of the superposition of wave-related and background currents and how this superposition interacts with particulate-matter properties and transport. Spatiotemporal wave-controlled patterns of particle dynamics seem to control spatiotemporal heterogeneity and could have consequences for the formation of the sedimentary record, for the benthic and benthopelagic community's food supply, and for concomitant behavioral responses of these communities.

## References

- ARMI, L., AND R. C. J. MILLARD. 1976. The bottom boundary layer of the deep ocean. *J. Geophys. Res.* **81**: 4983-4990.
- BARNETT, P. R. O., J. WATSON, AND D. CONNELLY. 1984. A multiple corer for taking virtually undisturbed samples from shelf, bathyal and abyssal sediments. *Oceanol. Acta* **7**: 399-408.
- BEAULIEU, S., AND R. BALDWIN. 1998. Temporal variability in currents and the benthic boundary layer at an abyssal station off central California. *Deep-Sea Res. II* **45**: 587-615.
- BIOSPHERICAL INSTRUMENTS. 1993. QSP-200L Log Quantum Scalar Irradiance Sensor—instruction manual.
- BOGUCKI, D. J., T. DICKEY, AND L. G. REDEKOPP. 1997. Sediment resuspension and mixing by resonantly generated internal solitary waves. *J. Phys. Oceanogr.* **27**: 1181-1196.
- CULLEN, J. J., AND M. R. LEWIS. 1988. The kinetics of algal photoadaptation in the context of vertical mixing. *J. Plankton Res.* **10**: 1039-1063.
- DR. HAARDT OPTIK MIKROELEKTRONIK. 1996. Manual BackScat II—fluorometer, model 1303 MP/CHIA/Phy/2R/MO.
- FOWLER, S. W., AND G. A. KNAUER. 1986. Role of large particles in the transport of elements and organic compounds through the oceanic water column. *Prog. Oceanogr.* **16**: 147-194.
- GARDNER, W. D. 1977. Incomplete extraction of rapidly settling particles from water samplers. *Limnol. Oceanogr.* **22**: 764-768.
- GLOOR, M., A. WÜEST, AND D. M. IMBODEN. 2000. Dynamics of mixed bottom boundary layers and its implications for diapycnal transport in a stratified, natural water basin. *J. Geophys. Res.* **105**: 8629-8646.
- , ———, AND M. MÜNNICH. 1994. Benthic boundary mixing and resuspension induced by internal seiches. *Hydrobiologia* **284**: 59-68.
- GRAF, G. 1992. Benthic-pelagic coupling: A benthic view. *Oceanogr. Mar. Biol. Ann. Rev.* **30**: 149-190.
- GRANATA, T., J. WIGGERT, AND T. DICKEY. 1995. Trapped, near-inertial waves and enhanced chlorophyll distributions. *J. Geophys. Res.* **100**: 20793-20804.

- GROSSART, H. P., AND H. PLOUG. 2001. Microbial degradation of organic carbon and nitrogen on diatom aggregates. *Limnol. Oceanogr.* **46**: 267–277.
- IMBERGER, J. 1998. Flux paths in a stratified lake: A review, p. 1–18. *In* J. Imberger [ed.], *Physical processes in lakes and oceans*. Coastal and Estuarine Studies. American Geophysical Union.
- JEFFREY, S. W. 1997. Application of pigment methods to oceanography, p. 127–166. *In* S. W. Jeffrey, R. F. C. Mantoura, and S. W. Wright [eds.], *Phytoplankton pigments in oceanography: Guidelines to modern methods*. UNESCO.
- , AND M. VESK. 1997. Introduction to marine phytoplankton and their pigment signatures, p. 37–84. *In* S. W. Jeffrey, R. F. C. Mantoura, and S. W. Wright [eds.], *Phytoplankton pigments in oceanography: Guidelines to modern methods*. UNESCO.
- KIEFER, D. A., AND R. A. REYNOLDS. 1992. Advances in understanding phytoplankton fluorescence and photosynthesis, p. 155–174. *In* P. G. Falkowski and A. D. Woodhead [eds.], *Primary productivity and biogeochemical cycles in the sea*. Plenum.
- KRAUSS, W. 1974. Interne Wellen, p. 77–84. *In* L. Magaard and G. Rheinheimer [eds.], *Meereskunde der Ostsee*. Springer-Verlag.
- LAMPITT, R. S., P. P. NEWTON, T. D. JICKELLS, J. THOMSON, AND P. KING. 2000. Near-bottom particle flux in the abyssal northeast Atlantic. *Deep-Sea Res. II* **47**: 2051–2071.
- LEIPE, T., A. LOEFFLER, L.-C. EMEIS, S. JÄHMLICH, R. BAHLO, AND K. ZIERVOGEL. 2000. Vertical patterns of suspended matter characteristics along a coastal-basin transect in the Western Baltic Sea. *Estuarine Coastal Shelf Sci.* **51**: 789–804.
- LENNERT-CODY, C. E., AND P. J. S. FRANKS. 1999. Plankton patchiness in high-frequency internal waves. *Mar. Ecol. Prog. Ser.* **186**: 59–66.
- , AND ———. 2002. Fluorescence patches in high frequency internal waves. *Mar. Ecol. Prog. Ser.* **235**: 29–42.
- MAGAARD, L. 1974. Wasserstandsschwankungen und Seegang, p. 67–75. *In* L. Magaard and G. Rheinheimer [eds.], *Meereskunde der Ostsee*. Springer-Verlag.
- MIDDELBURG, J. J. 1989. A simple rate model for organic matter decomposition in marine sediments. *Geochim. Cosmochim. Acta* **53**: 1577–1581.
- MOORE, L., R. GOERICKE, AND S. W. CHISHOLM. 1995. Comparative physiology of *Synechococcus* and *Prochlorococcus*: Influence of light and temperature on growth, pigments, fluorescence and absorptive properties. *Mar. Ecol. Prog. Ser.* **116**: 259–275.
- OLIVER, R. L., AND J. WHITTINGTON. 1998. Using measurements of variable chlorophyll-*a* fluorescence to investigate the influence of water movement on the photochemistry of phytoplankton, p. 517–534. *In* J. Imberger [ed.], *Physical processes in lakes and oceans*. Coastal and Estuarine Studies. American Geophysical Union.
- RIBBE, J., AND P. E. HOLLOWAY. 2001. A model of suspended sediment transport by internal tides. *Cont. Shelf Res.* **21**: 395–422.
- RICHARDS, K. J. 1984. The interaction between the bottom mixed layer and mesoscale motions in the ocean: A numerical study. *J. Phys. Oceanogr.* **14**: 754–768.
- . 1990. Physical processes in the benthic boundary layer. *Phil. Trans. R. Soc. London A* **331**: 3–13.
- RICKERT, D., M. SCHLÜTER, AND K. WALLMANN. 2002. Dissolution kinetics of biogenic silica from the water column to the sediments. *Geochim. Cosmochim. Acta* **66**: 439–455.
- RUTGERS VAN DER LOEFF, M. M., AND B. P. BOUDREAU. 1997. The effect of resuspension on chemical exchanges at the sediment–water interface in the deep sea—a modelling and natural radiotracer approach. *J. Mar. Syst.* **11**: 305–342.
- SEIFERT, T., AND B. KAYSER. 1995. A high resolution spherical grid topography of the Baltic Sea. Marine Science Reports. Institut für Ostseeforschung Warnemünde.
- SIEDLER, G., AND G. HATJE. 1974. Temperatur, Salzgehalt und Dichte, p. 43–60. *In* L. Magaard and G. Rheinheimer [eds.], *Meereskunde der Ostsee*. Springer-Verlag.
- SMETACEK, V. 1980. Annual cycle of sedimentation in relation to plankton ecology in Western Kiel Bight. *Ophelia Suppl.* **1**: 65–76.
- , K. v. BROECKEL, B. ZEITZSCHEL, AND W. ZENK. 1978. Sedimentation of particulate matter during a phytoplankton spring bloom in relation to the hydrographical regime. *Mar. Biol.* **47**: 211–226.
- THORPE, S. A. 1983. Benthic observations on the Madeira Abyssal Plain: Fronts. *J. Phys. Oceanogr.* **13**: 1430–1440.
- TURNEWITSCH, R., AND B. M. SPRINGER. 2001. Do bottom mixed layers influence  $^{234}\text{Th}$  dynamics in the abyssal near-bottom water column? *Deep-Sea Res. I* **48**: 1279–1307.
- VERARDO, D. J., P. N. FROELICH, AND A. MCINTYRE. 1990. Determination of organic carbon and nitrogen in marine sediments using the Carlo Erba NA-1500 Analyzer. *Deep-Sea Res.* **37**: 157–165.
- WANG, B.-J., D. J. BOGUCKI, AND L. G. REDEKOPP. 2001. Internal solitary waves in a structured thermocline with implications for resuspension and the formation of thin particle-laden layers. *J. Geophys. Res.* **106**: 9565–9585.
- WÜEST, A., AND M. GLOOR. 1998. Bottom boundary mixing: The role of near-sediment density stratification, p. 485–502. *In* J. Imberger [ed.], *Physical processes in lakes and oceans*. Coastal and Estuarine Studies. American Geophysical Union.

Received: 22 April 2002  
Accepted: 7 January 2003  
Amended: 22 January 2003